2

E7.6-10153

NASA CR-144504
ERIM 102000-42-F

Final Report

ASSESSMENT OF MAPPING EXPOSED FERROUS AND FERRIC IRON COMPOUNDS USING SKYLAB-EREP DATA

H. WAGNER, W. PILLARS, R. VINCENT, and C. BENNETT
Infrared and Optics Division

JANUARY 1976

Prepared for
NATIONAL AERONAUTICS AND SPACE ADMINISTRATION

Johnson Space Center
Houston, Texas 77058
Contract NAS9-13317
Technical Monitor: L. B. York, TF6

ENVIRONMENTAL
RESEARCH INSTITUTE OF MICHIGAN
FORMERLY WILLOW RUN LABORATORIES, THE UNIVERSITY OF MICHIGAN
BOX 618 • ANN ARBOR • MICHIGAN 48107

TECHNICAL REPORT STANDARD TITLE PAGE

1. Report No.	2. Government Accession No.	3. Recipient's Catalog No.
NASA-CR-ERIM 102000-42-F		

4. Title and Subtitle	5. Report Date
ASSESSMENT OF MAPPING EXPOSED FERROUS AND FERRIC IRON COMPOUNDS USING SKYLAB-EREP DATA	January 1976
	6. Performing Organization Code

7. Author(s)	8. Performing Organization Report No.
H. Wagner, W. Pillars, R. Vincent, and C. Bennett	102000-42-F

9. Performing Organization Name and Address	10. Work Unit No.
Environmental Research Institute of Michigan P.O. Box 618 Ann Arbor, Michigan 48107 (313) 994-1200	11. Contract or Grant No. NAS9-13317
12. Sponsoring Agency Name and Address	13. Type of Report and Period Covered
National Aeronautics and Space Administration Johnson Space Center Houston, Texas 77058	Final Report 8 March 1973 – 30 August 1975
	14. Sponsoring Agency Code

15. Supplementary Notes

16. Abstract

The utility of S190B color photography and machine processed S192 data for mapping exposed ferrous and ferric iron compounds was assessed in a test area near Pisgah Crater, California. Maps of various colors of rocks and alluvium were made using S190B photography collected on 26 January 1974. Red and near infrared channels of S192 were machine processed by dark level correction and ratio processing. Resultant maps, displayed in color coded form, were compared with the S190B photointerpretive map and with a single band color coded density sliced map.

A separate experiment assessed the utility of S191 data to separate basalt and dacite on the basis of reststrahlen features in the 8 – 12 μm range.

Original photography may be purchased from:
EROS Data Center
10th and Dakota Avenue
Sioux Falls, SD 57198

ORIGINAL CONTAINS
COLOR ILLUSTRATIONS

17. Key Words	18. Distribution Statement
Geologic Remote Sensing Skylab Earth Resources Experiment Multispectral Scanner Satellite Photography Computer Processing	Initial distribution is listed at the end of this document.

19. Security Classif. (of this report)	20. Security Classif. (of this page)	21. No. of Pages	22. Price
Unclassified	Unclassified	65	

PREFACE

This report concludes investigations in geologic remote sensing from March 1973 through June 1975. The research described in this report was performed under Contract NAS9-13317 Skylab-EREP Investigation 444M. All of the work was done at the Environmental Research Institute of Michigan (formerly Willow Run Laboratories of the University of Michigan), in the Infrared and Optics Division, headed by R. R. Legault. The principal investigators were Robert K. Vincent; Principal Investigator from 8 March 1973 through 30 September 1974 and Frederick J. Thomson; from 1 October 1974 through 30 August 1975. Robert K. Vincent was an Associate Research Geophysicist at ERIM's Infrared and Optics Laboratory (presently of Geospectra Corporation, Ann Arbor, Michigan). Frederick J. Thomson is a Research Engineer at ERIM's Infrared and Optics Laboratory. The Technical Monitor for this investigation was Larry B. York.

The purpose of this investigation was (a) to determine the feasibility of using ratio techniques to map iron compounds on the exposed surfaces of rocks and soils and to differentiate silicate rock types, and (b) to demonstrate the feasibility of using satellites with a multi-band thermal infrared capability to map inaccessible areas of the world.

The collection date was to have originally been in September 1973 and the data was to have been delivered in January 1974. The data were collected on 26 January 1974 and delivered to ERIM in November and December 1974. The main technical effort on this investigation was thus delayed until early 1975. S190A color photography, S192 computer compatible tapes of calibrated data and corresponding screening film, and S191 computer compatible tapes of digitized data were used in this investigation.

We would like to acknowledge the assistance of Mr. Harvey Wagner (computer processing) and Miss Debbie Compton and Mrs. Nancy Moon.

CONTENTS

FIGURES

TABLES

ASSESSMENT OF MAPPING EXPOSED FERROUS AND FERRIC IRON COMPOUNDS USING SKYLAB-EREP DATA

1 INTRODUCTION

This is the final report on Contract NAS9-13317 dealing with the use of Skylab-EREP data to map ferrous and ferric iron compounds and to map silicate minerals. S190B, S191, and S192 data were analyzed. The S190B and S192 data were used for ferrous and ferric iron compound mapping, while the S191 data was used for assessment of the feasibility of mapping silicate minerals from space. The test site used for these investigations was near Pisgah Crater, California — an area extensively studied in the past and one with large extent of exposed iron-containing materials.

This investigation was conducted between 8 March 1973 and 30 August 1975, with intensive effort after the receipt of S191 and S192 data from the 26 January 1974 overpass during the SL4 mission.

1.1 SCOPE OF STUDY

This study was to evaluate the Skylab-EREP data for mapping ferric and ferrous iron compounds and for mapping silicate minerals. The ability of EREP data to map iron compounds was to be compared with the ability of ERTS (LANDSAT) to map these compounds. The feasibility of mapping silicate minerals using the thermal infrared ratio technique developed by Vincent and Thomson [1] was to be assessed using S191 data.

Section 4 presents a discussion of the work on iron compounds. Section 5 presents the work on silicate mineral mapping potential. Section 6 presents conclusions and recommendations specifically

addressing the comparison of various EREP sensors with the ERTS (LANDSAT) MSS, and recommending parameters for future spacecraft sensors.

1.2 APPROACH

The approaches to both the iron compounds mapping study and the silicate mapping study were similar. A review of previous work (summarized in Section 2) was followed by modelling to determine the optimum spectral ratios for mapping iron compounds with Skylab S192 data. Since not all spectral channels of information necessary to compute the most favorable ratios were available in our limited SL4 data set, ratios of red to infrared and infrared to infrared bands were formed. Because of the limited spectral band set available from S192, an exhaustive comparison of S192 and LANDSAT capabilities to map iron compounds was not possible.

The approach to the assessment of silicate mineral mapping (using reststrahlen features of silicate minerals in the 8 - 14 μm region) was to examine S191 data of dacite and basalt collected over the Pisgah Crater site on 26 January 1974. After correcting the data for atmospheric absorbtion and path radiance (calculated from a model), the utility of two and three band ratio techniques for discriminating these rock types was assessed. Two pairs were examined — the optimum 0.5 μm wide bands derived by Vincent [2] and the 1 μm wide bands of the Surface Composition Mapping Radiometer (SCMR). Suggested parameters for a spacecraft sensor were derived from these two band pairs. The impact of adding a third band to make temperature corrections was assessed.

1.3 SUMMARY OF CONCLUSIONS

As a result of this investigation, several conclusions were drawn. They are summarized here and more fully discussed in Section 6 of this report.

1. As a result of our studies, we feel that the S190B color photography is at least as useful as LANDSAT data for the mapping of color differences in the rocks and soils of and terrain. There is hope that the S190B color film with its blue sensitive emulsion might be able to discriminate between tan and yellow colored rock samples — an important distinction for some geologic mapping problems and one which cannot be done from LANDSAT data. Compared with LANDSAT data, the superior spatial resolution of S190B color photography will also allow a more reliable mapping of colors (through the joint use of textural features) and the more precise delineation of faults and linears.

2. Spectral ratio images, using pairs of bands suggested by analysis of ratio codes derived from laboratory spectra, form a valuable data set for the reconnaissance mapping of geologic areas. The ratio maps must be properly interpreted and used in conjunction with other sources of information to be of information to be of greatest use.

3. A detailed comparison of the S192 and LANDSAT ratio capabilities was not possible because data from only eight of the thirteen S192 bands were delivered. An S192 ratio of 0.79 - 0.89 and 0.93 - 1.05 μm bands produced an apparently successful delineation of ferrous, ferric, and other materials, in agreement with theory and ratio code studies. It is recommended that bands in this region be considered for future sensors for geologic applications.

4. We found, from an analysis of S191 data that basalt and dacite could be separated on the basis of differences in spectral emissivity in the 8.3 - 12 μm region. Half micron wide bands (8.3 - 8.8 and 10.3 - 10.8 μm), indicated as optimum by previous studies, would give reliable separation with a system noise equivalent temperature (NET) of 1.2°K or less, while the bands used in the Surface Composition Mapping Radiometer (SCMR) (8.3 - 9.3 and 10.2 - 11.2 μm) required a 1.1°K or less NET for adequate separation. We assumed that a channel in the 12 μm region would be available for temperature correction.

2
PREVIOUS WORK

There has been a variety of laboratory, theoretical, and empirical work done on both the iron compounds and silicate minerals mapping using remote sensing techniques.

Theoretical studies have been used to indicate what geochemical factors dominate spectra in specific wavelength regions. Work done in the near infrared region (0.8 - 2 μm) has indicated that ferric and ferrous iron absorption and absorbtion by water are important features of the reflectnace spectra in that region. Optical absorption caused by electronic transitions of the ferrous and ferric ion results in broad reflectance minima in the visible and near infrared spectra of iron-bearing minerals. Rowan [3] found that reflectance minima in the near-infrared spectra for materials containing minor amounts of iron are generally less pronouned than the reflectance minima measured for iron-rich minerals in the near-infrared region.

Rowan and others have used ratio processed, color coded LANDSAT data to investigate a hydrothermally altered area in Nevada [11]. Using three ratios of ERTS bands (MSS4/MSS5, MSS5/MSS6, and MSS6/MSS7) they were able to isolate areas where hydrothermal alteration had occurred. The mapping accuracy was not perfect because some areas showing ratio values indicative of alteration were not altered and some hydrothermally altered areas did not show ratio values indicative of the alteration in other areas. At least one key to the ability to map the altered areas was the presence of limonite, a red-brown ferric oxide. Other non-ferrous alteration minerals such as Kaolinite, alunite, montmorillonite, and jarosite, could not be separated from limonite. Rowan hypothesized that bands available in S192 beyond 1.1 μm, and greater spectral resolution in the 0.8 - 1.1 μm region would help separate these minerals.

Infrared coverage of the LANDSAT (0.7 - 0.8 and 0.8 - 1.1 μm) multispectral scanner is relatively wideband and not optimal for ferric and ferrous determinations. Channel MSS7 covers both the ferrous and ferric absorption bands (at 1.0 and 0.95 μm respectively) so that no differentiation between these two materials can be made. Use of channel 7 to separate iron-rich materials from other materials is also hampered by the broad bandwidth of the MSS7 band. Skylab S192 bands provide for better separation of specific absorption peaks. Channel 7 of LANDSAT is broken up into three bands in the S192 multispectral scanner; band 7 covers the .77 to .89 μm wavelength region, band 8 ranges from .93 to 1.05 μm, and band 9 covers the region from 1.03 to 1.19 μm. In addition to those channels overlapping LANDSAT infrared coverage, the S192 provides two bands farther into the reflective infrared (1.55 - 1.75 and 2.05 - 2.35 μm). These two bands are of particular interest because they are out of the region available to photographic processing.

In a study using a 12 channel aircraft scanner to simulate the Skylab S192 information, Pohn [4] reports the presence of high reflectance anomalies in the near-infrared. Missions were flown over six areas believed to be representative of the major geologic units in the southwestern Nevada-southern California Skylab test site. Anomalies exhibiting moderately high reflectivity in wavelength region 2.0 - 2.6 μm were observed in the images from the aircraft mission for several areas, including an area east of Pisgah Crater. Similar anomalies in Skylab S192 images of the Nevada test site appear in Skylab band 11 (1.55 - 1.75 μm), but not in images at wavelengths less than 1.0 μm (band 7, 0.78 to 0.88 μm).

Both in the aircraft and the Skylab imagery, the anomalies are almost always in reddish volcanic rocks which are at least as mafic as andesite, and are mapped as Teritary or younger. However, the spectra of most of the andesite and the spectra of more mafic rocks

in these areas do not show anomalous infrared reflections. Pohn found that in examining the spectral curves of Hunt and others for common intermediate and mafic rocks, the reflectivity of the oxides hematite, goethite, and limonite shows an increase near the infrared. Only in the smallest particle size range (0-5 μm) do the curves approach the very high reflectivity of the anomalies. That grain size is an important factor in the recognition of the iron oxides is indicated by the spectral curves.

It has been suggested by Ray Wilcox and Richard White of the U. S. Geological Survey that the late eruptive oxidation of mafic minerals and precipitation of sublimate during posteruptive fumarolic steaming produces the iron oxides. Pohn determined that a reasonable explanation of the anomalies is that the anomalous materials have a 5 μm or finer coating of hematite that formed during the posteruptive fumarolic steaming and the cooling.

Hunt, Salisbury, and Lenhoff [5,6,7], examining the bidirectional reflectance spectra of igneous rocks for a wavelength region of 0.325 - 3.5 μm, found that in acidic and intermediate igneous rocks, most spectral features occur as a result of the presence of iron, hydroxyl and water. Therefore, these spectral features are only indirect indicators of composition. Acidic rocks contain minerals that are mostly spectrally featureless, their light color resulting in a high overall reflectivity. The intensity of the water and hydroxyl features displayed in acidic rock spectra near 1.4, 1.9, and beyond 2.3 μm is due to water in fluid inclusions common in the relatively low temperature felsic minerals, the high transparency of these minerals, and to the common late stage alteration of felsic minerals. The only spectral features commonly found in basic rock spectra are those due to iron near 1.0 μm, and these features are normally weak and broad. The hydroxyl 1.4 μm and water 1.9 μm features occur very rarely, but are present only as a result of weathering or alteration

of the rock. Because of the large amounts of dark mafic minerals, particularly magnetite and other opaque minerals, basic rocks have the lowest reflectivities of any rocks, with the exception of very light colored anorthosite gabbros. Ultra-basic rocks display strong ferrous iron bands near 1.0 μm, and near 1.7 - 2.0 μm.

In an assessment of the utility of the visible and near-infrared region for remote sensing of rock type, Salisbury and Hunt [8] determined that compositionally diagnostic spectral signatures are not displayed by many of the important rock-forming minerals in this wavelength region. Rocks composed primarily of minerals lacking diagnostic spectral signatures may yield featureless spectra or their spectrum may be dominated by the spectral features of minor constitutents or alteration products. These spectral features would be indirectly related to the primary mineralogy. Opaque minerals which are contained by many rocks may influence the reflectance spectrum of a rock by reducing spectral features and the overall reflectivity. Another problem in examining the spectra of rocks in the visible and near-infrared region is that atmospheric absorption bands may obscure some of the spectral features that are most important in rock type discrimination using remote sensing.

Vincent [1,9] determined that important spectral features of geologic materials, related primarily to interatomic phenomena, occur at wavelengths longer than 2.0 μm. Characteristic spectral emittance minima in the 8.0 μm to 14 μm region are produced by interatomic vibrations in silicate minerals. Information concerning chemical composition and structure of the minerals is contained in these spectral emittance minima. Depending on their mineral assemblages, igneous rocks may also display characteristic spectral emittance minima in the 8.0 to 14 μm wavelength region. In this region, the effect of rock composition on spectral emittance will most likely not be masked by variations of texture common to silicate rocks as a result of their

formation. The textural effects on spectral emittance can be larger for carbonate rocks.

Generally, Vincent [9] found that the emittance minima for mafic and ultramafic rocks occur at longer wavelengths than emittance minima of felsic rocks. Figure 1 is a rearranged plot of Lyon's (1964) data [10] showing the emittance spectra of 25 silicate rocks of varying SiO_2 content from approximately 35 to 68%. Emittance minima for under-saturated rocks, such as nepheline syenite, occur near the middle of the felsic-ultramafic extremes.

In a study to choose the optimal filter combination for implementation of a two-channel thermal infrared ratio method on low altitude aircraft scanner data, Vincent (1974) selected 8.1 - 10.1 μm and 9.2 - 11.2 μm. Atmospheric model corrections applied to low altitude data allow simulation of satellite data. On the basis of this preliminary theoretical work and with the availability of the S191 spectrometer, study of the feasibility of general geologic mapping is a tractable problem.

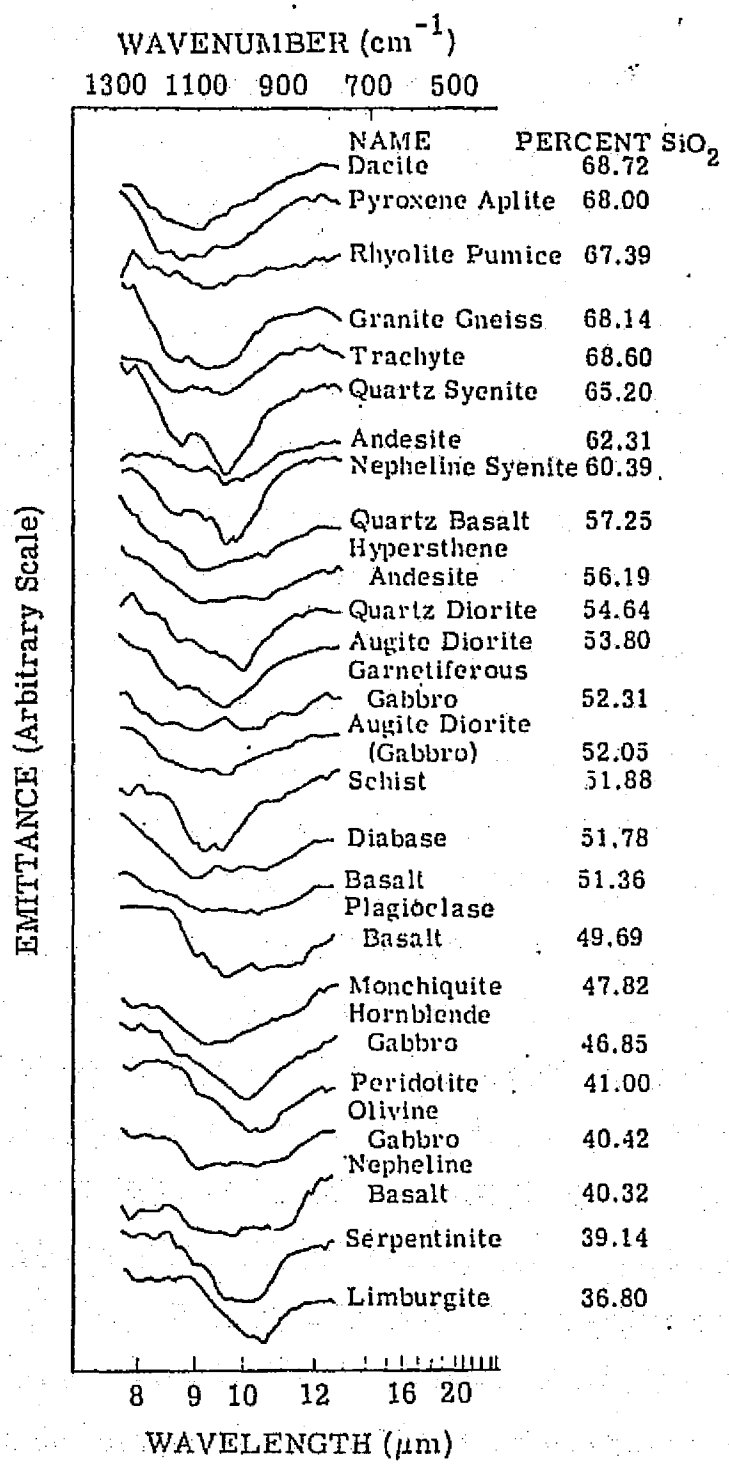

FIGURE 1. EMITTANCE SPECTRA OF SILICATE ROCKS (after Lyon 1964)

3

GENERAL INTRODUCTION TO THE GEOLOGY OF THE PISGAH CRATER AREA

The Pisgah Crater region in San Bernadino County, California is located in the Basin and Range physiographic province. It is one of the many centers of recent volcanic activity which lie on broadly alluviated valleys and playas across the central part of San Bernadino County in the southern Mojave Desert (Figure 2). The study area is approximately 36 miles to the northeast of the San Andreas fault system, and the length of the study site runs in an almost parallel direction (to the northwest) with it. The study area is extensively faulted by a series of almost parallel faults running in a northwest direction. The climate is semi-arid, and the volcanic terrain is sparsely vegetated.

The valley fill material of the study region is made up of nonmarine sedimentary deposits of Pleistocene age, Recent alluvium, dune sand, and playa lake deposits. The Pleistocene nonmarine sediments are undeformed to slightly deformed, dissected alluvial fan deposits. Gravel, sand, and silt of these deposits has been locally cemented by caliche. The alluvial deposits of Pleistocene to Recent age, consisting of coarse gravel bordering the mountains, grade into pebble gravel and sand in the valley areas. Locally there are dunes of loose, fine sand deposited by the prevailing westerly winds. The Recent playa lakes are made of fine micaceous silt and clay. The top surfaces of these lakes are level.

The Big Horn Mountains and Little San Bernadino Mountains in the southwestern area of the study region are composed mostly of Mesozoic granite to quartz monzonite, biotite quartz monzonite, granodiorite, and Precambrian gneiss. The granite to quartz monzonite group is felsic, fresh, hard, massive, and composed of fine to medium grained

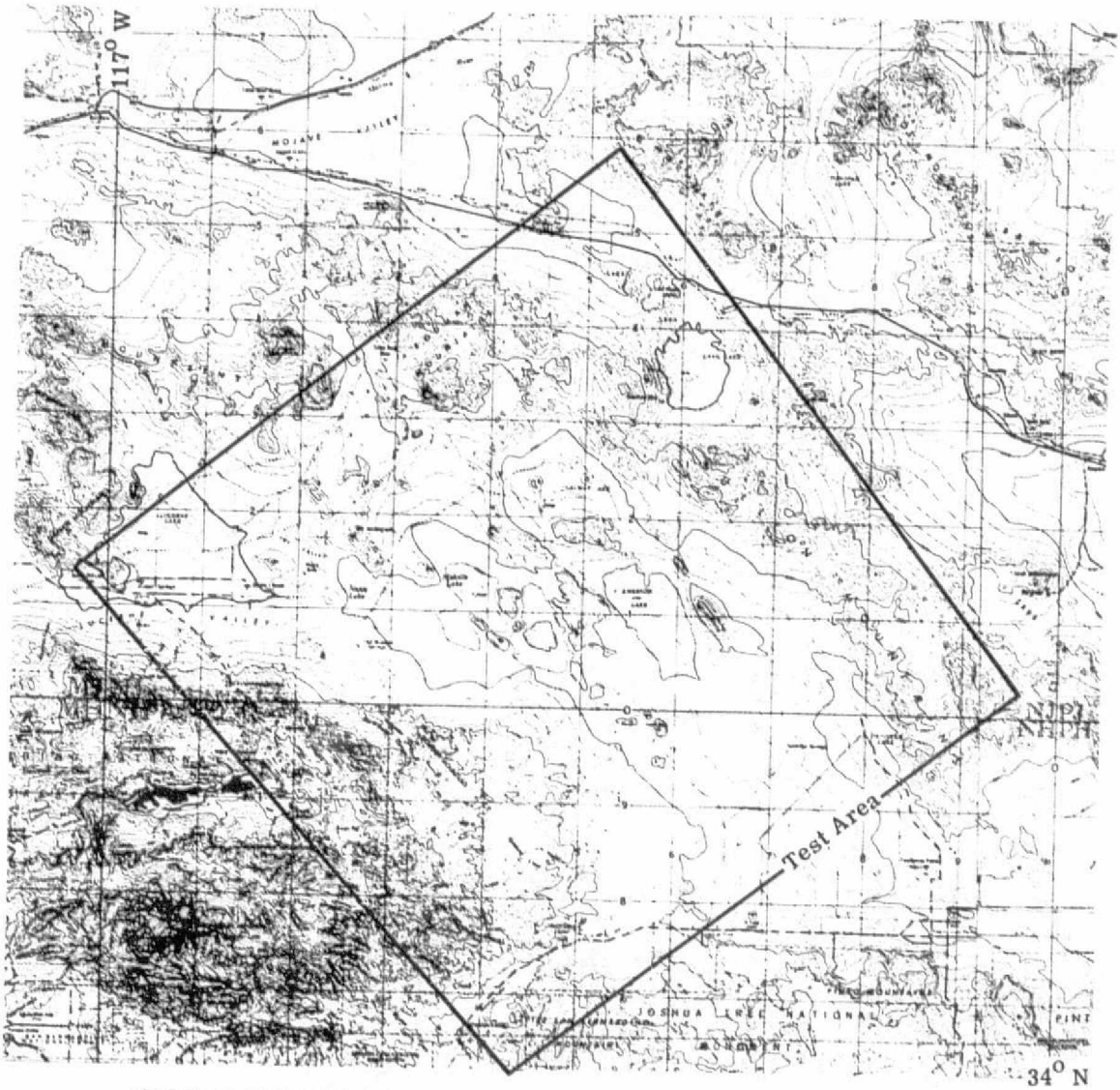

FIGURE 2. MAP OF PISGAH CRATER TEST SITE

quartz, orthoclase, and plagioclase in about equal proportions, with 1-2% biotite. The 0-1% hornblende present is locally partly chemically weathered to brown iron oxides. The monzonite is about 1% iron oxides. The biotite quartz monzonite is gray, massive, hard, medium grained, and is composed of quartz, orthoclase, and plagioclase in nearly equal proportions. It contains biotite (5-20%) in clusters which have been altered to iron oxides, imparting a brown iron staining to the weathered rocks. The granodiorite is a light-gray and contains quartz (30%), orthoclase (10-20%), and plagioclase (40-50%) with less than 1% iron oxides. The Precambrian gneiss contains quartz, plagioclase, orthoclase, and biotite. It is a light gray, medium to fine grained granitic gneiss. In several places in the Big Horn Mountains, within the study area, there are Pliocene or early Pleistocene basalt intrusives. They are made up of a black, massive, non-vesicular basalt. The basalt contains scattered small phenocrysts of olivine and plagioclase in a microcrystalline groundmass of plagioclase laths, green pyroxene(?), and specks of magnetite.

Most of the rock outcrops in the main valley are a quartz to biotite quartz monzonite, similar to the monzonites in the Big Horn and Little San Bernadino Mountains. Into these monzonite outcrops, there are areas of intrusives of biotite diorite. The biotite diorite is a dark gray and composed mostly of calcic plagioclase and biotite with small amounts of hornblende, chlorite, and iron oxides.

The Fry and Rodman Mountains in the northern section of the study area are mostly made up of quartz monzonite and biotite quartz monzonite similar to the quartz and biotite quartz monzonites of the Big Horn and Little San Bernadino Mountains, with 2-5% biotite in the quartz monzonite and 5-20% biotite in the biotite quartz monzonite. The basalt of the Malpais Crater is a black, hard, vesicular, fine-grained basalt. It contains small phenocrysts of olivine in a fine-grained groundmass of labradorite, pyroxene, and magnetite. There are

several small local deposits of iron oxides in these mountains. The iron oxides are a black to dark greenish brown massive iron ore, composed of magnetite and hematite.

The Lava Bed Mountains and Bullion Mountains are made up of several basalts, andesite, tuff breccia, rhyolitic felsite, dacite porphyry, and biotite quartz monzonite. The basalt of the Sunshine flow is a vesicular, hard, black basalt composed of gray plagioclase, basaltic glass, and small amounts of pyroxene, olivine, and magnetite. The basalt of the Lava Bed Mountains is a black, massive, hard basalt composed of calcic plagioclase and pyroxenes. It contains finely divided iron oxides. The basalt of the Bullion Mountains is dark gray to black, occurring in masses to thickly layered flows. It is composed of microlitic calcic plagioclase and pyroxene with grains of plagioclase and magnetite. The andesite of these mountains is massive, and pinkish to greenish gray. It is a groundmass of mostly plagioclase containing phenocrysts of white plagioclase (making up from 20-50% of the rock mass), some biotite flakes, needles of hornblende, and specks of iron oxides. The tuff breccia of this area is a tan to a gray white, and is composed of small white fragments of pumice to angular fragments of felsitic andesitic rocks in a matrix of fine to coarse grained tuff. Also present in the Bullion Mountains is a rhyolitic felsite. It is a light-brown-gray, massive, hard, fine grained felsite. It contains small phenocrysts of sodic plagioclase, sanadine, quartz, and flakes of biotite. The southern extension of the Bullion Mountains is mostly biotite quartz monzonite. It is a gray, massive, commonly porphyritic granitice rock that is 3-20% biotite. The biotite is often altered to iron oxides. There is a large dacite porphyry located to the west and southwest of the Sunshine lava flow. This is a gray-white to light greenish gray, massive porphyry. It contains phenocrysts of white plagioclase, biotite, and hornblende, (making up 40 to 60% of the rock mass), in a

groundmass of plagioclase and orthoclase. There are trace amounts of iron oxides, and there has been a fair amount of altering of dark minerals to iron oxides.

Further ground truth information concerning the area is available in other reports and geologic maps [11-18].

4

IRON COMPOUNDS MAPPING

There is ample evidence from previous work on both ERTS and photographic data that red or brown areas sometimes indicative of iron compounds can be mapped in arid, spasely vegetated terrain. Basically, three techniques can be used — photointerpretation, single channel multispectral scanner signal slicing, and spectral ratio processing. The spectral ratio processing can be performed using both visible and near infrared bands.

In this section, we discuss these three types of processing and results obtained when they were applied to Skylab-EREP data. An analysis of the information content of these images is presented and comparisons with ERTS results are made.

At the outset, two limitations of the Skylab data set, both relating to the S192 data, should be mentioned. Data were collected over the Pisgah Crater site in late January 1974. At that time, the S192 sensor had a detector array which was optimized for thermal (10.4 - 12.5 μm) data acquisition. Consequently, data for the visible and near infrared channels were degraded by excessive noise and overshoot (the latter caused by improper frequency response match between the detectors and preamplifiers). Through digital filtering of conical scan tapes, we were able to improve the quality of some of the red and near infrared bands to a point where processing could continue. Some visible bands (e.g., channels 1-5 covering 0.42 - 0.65 μm) could not be improved sufficiently and were discarded from further analysis. This largely precluded any comparison with ERTS data.

Second, because of orbit drift, the track of earlier Skylab passes had not covered Pisgah Crater. Also the S192 coverage of the late January pass was marginal. The failure of earlier passes to cover

the test site convinced other investigators to move their investigations to other test sites. We had unofficial arrangements with these investigators to share some of their ground information. Also because the coverage of the area was not what was originally anticipated, ground information we had collected as part of previous investigations was not optimally useful. Both these factors compromised the quality of results obtained.

4.1 S190B PHOTOGRAPHY INTERPRETATION AND ANALYSIS

A color interpretation was performed on an S190B photograph of the area to allow an indirect comparison with LANDSAT capabilities.

The color interpretation was done with the use of a light table and a zoom-transfer scope. One frame covering the study site was examined. The examination was based solely on color and color variations in the scene. Using the zoom-transfer scope, an interpretive map of the study site was made. This map indicates the main boundaries between some rock formations and their detritus and the color boundaries as interpreted in the S190B photograph.

The study area is made up mostly of granitic and volcanic rocks. The basalt flows in the region are very distinct in the S190B image because of their dark color. Contacts between volcanic and granitic rocks are visible. In the S190B photograph, there is little distinction among the types of granitic rocks. Much of the rock outcrop and detrital material in the area are a red color that is probably due to the deposition of iron oxides weathered from iron rich rocks. There are several playa lake deposits in the Pisgah Crater study area which appear very bright in the photograph. Some zonation is observed in the Emerson Lake playa deposit.

Figure 3 is the S190B photograph of the Pisgah Crater area study site. Figure 4 is an interpretive map drawn from the S190B image with the use of a zoom-transfer scope. The heavy dark lines indicate

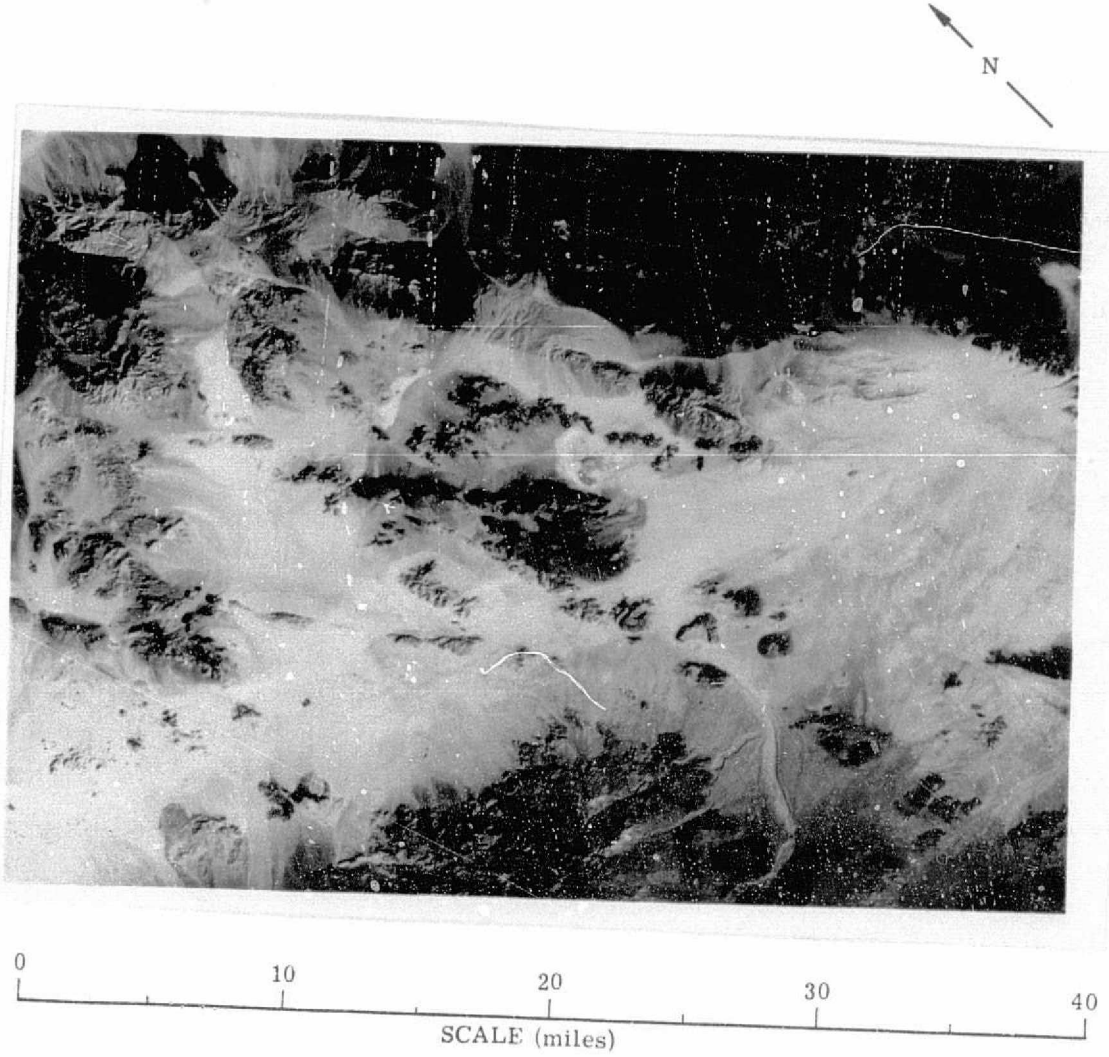

FIGURE 3. S190B IMAGERY OF PISGAH CRATER TEST SITE, 26 JANUARY 1974, 1940 hrs GMT

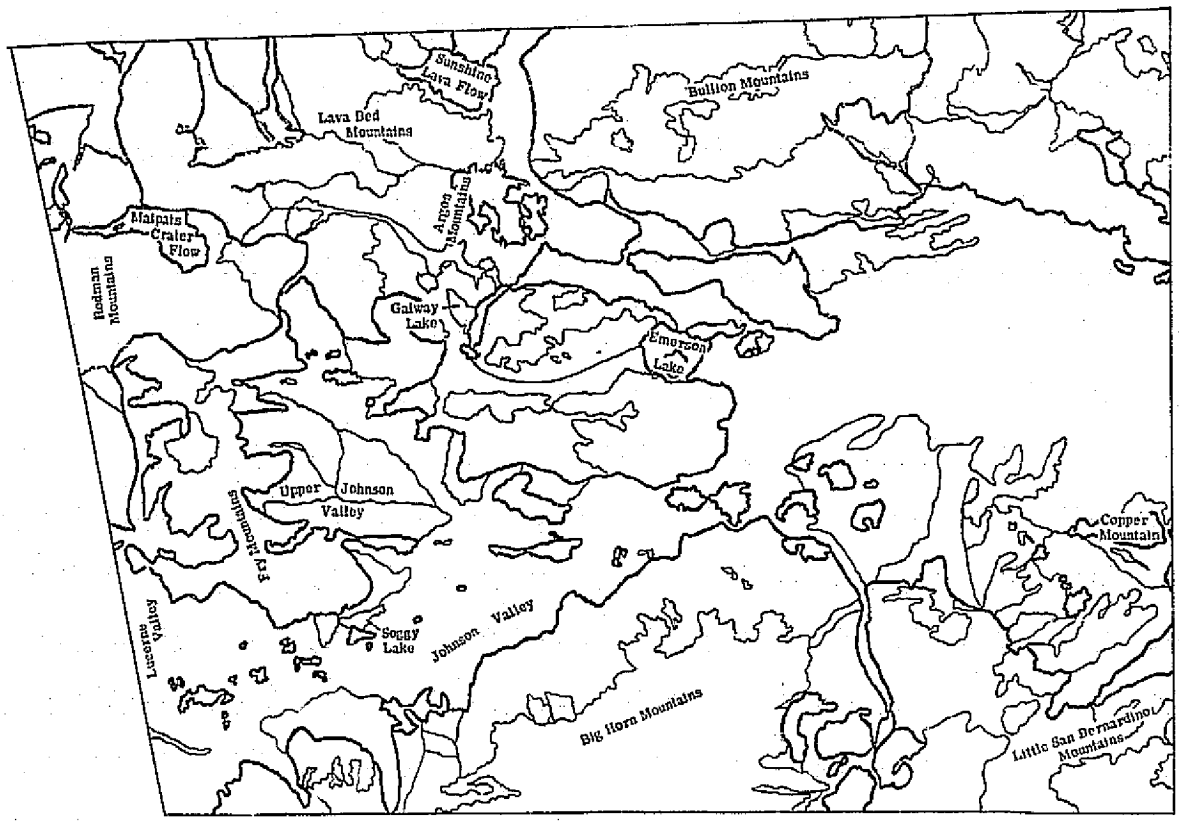

FIGURE 4. MAP SHOWING MAJOR AND MINOR COLOR BOUNDARIES OF THE PISGAH CRATER TEST SITE, AS INTERPRETED FROM S190B PHOTOGRAPHY, 26 JANUARY 1974 GMT

interpreted major boundaries between surficial materials. The finer lines indicate minor divisions within the materials. This interpretive map was drawn from information based primarily on color in the image, with some image texture information entering in the interpretation. Because of their dark color, the basalt flows are the most outstanding rock features in the image. The Sunshine Crater flow near the eastern edge of the study area is made up of basalt lava and basalt pumice [14]. There is some differentiation in the basalt flow that is visible in the imagery. The Malpais Crater flow is entirely basalt lava [13] and is similar in color to the Sunshine lava flow. Just to the southeast of the Malpais Crater flow is a trianular shaped region of basalt, andesite, and dacite [13]. In the imagery, this region is lighter in color than the other basalt flows. The andesite and dacite might explain this color difference. The drainage and detritus from the basalt-andesite-dacite outcrop is lighter gray than the main rock; the drainage from the outcrop is to the north-northeast. In the photography, the boundary between the rock outcrop and its detrital material can be determined. In the Lava Bed Mountains, near Argos Mountain, there is a very dark basalt which lies unconformably over a tuff breccia This basalt is discernable in the imagery but it is not as outstanding as the Sunshine or Malpais flows.

The Bullion Mountains are Miocene volcanics at the northern end of the range, and Mesozoic granitic rocks at the southern end of the range [14]. The contact between the volcanics and the granitic rocks is very distinctive in the photography. The volcanics are lighter in color than the basalt flows in the northern section of the study area. There are areas of very light rock in the volcanics. According to the geologic maps [14,15]. this volcanic group is made up of basalt, andesite, and intrusive felsite. The lighter color is probably a result of the andesite and felsite being present. In the photography, the volcanics of the Bullion Mountains and their detritus have a red

cast to them. The red color is probably due to the weathering of magnetite grains and biotite flakes contained in the basalt and andesite. According to the geologic maps, iron oxides are also present in the andesite. The granitic rocks of the Bullion Mountains are reported to be mostly biotite-quartz monzonite containing abundant biotite clusters and less than 2% iron oxides [15]. In the imagery, the granitic rocks of the southern Bullion Mountains have a reddish color that is probably due to the weathering of the biotite and the presence of iron oxides in the rock. The detritus from the grantic rocks of the Bullion Mountains into the southeast extension of Johnson Valley is very light in color, nondistinguishable from the main valley fill.

The Rodman Mountains in the northern section of the study region are biotite-quartz monzonite, quartz latite, and biotite diorite [13]. In the photography, there is no visible distinction between rock types. According to the geologic map, the biotite-quartz monzonite is 5-20% biotite, with some of the biotite altering to limonite. The quartz latite has much reddish-brown iron staining along fractures [13]. There is a discernable difference between the detritus and the parent material. The detritus is a red-gray, probably as a result of the weathering of biotite and iron oxides.

The Big Horn and Little San Bernadino Mountains are mostly quartz monzonite, granodiorite, and granitic gneiss [16,18]. In the imagery, there is no visible distinction between the rock types and the boundary between the parent rocks and detrial material is indistinct. The rocks have a reddish cast and the detritus is a red-gray. Based on information in the geologic map [18], most of the red color of both the rock and detritus is probably a result of the weathering of biotite and the alteration of biotite to iron oxides. In the west side of the study site, in the Big Horn Mountains, there are four basalt flows. The basalt flows are a dark red-brown and the detritus from these flows is a very bright red. The basalt contains specks of magnetite [17] which, when weathered, would impart the strong red color observed.

There is a main valley which extends from the northwest corner to the southcentral area of the study region. The valley material is light tan with some interlacing of red drainage materials. Most of the valley fill consists of nonmarine sedimentary deposits [16]. The red coloration of some of the drainage patterns in the valley fill appears to be a result of the deposition of weathering products of iron containing rocks. Some areas of the valley fill are very light in color. This very light color may be due to a thin coating of caliche or other evaporation deposits on the sediment materials. There are also some windblown sand deposits in the valley [18] which would appear very light in color.

The playa lake deposits of Emerson Lake, Soggy Lake, and Galway Lake all stand out in the photography as the brightest and lightest areas of the scene. According to the geologic maps [16,18], these playas are made up of a micaceous clay and silt. In the photography, there is some structure and differentiation in the Emerson Lake deposit. Zonation due to different lake levels is observed along the lake edge. Three color regions in Emerson Lake are visible. These different color regions may be due to material, chemical, or moisture differences. The lightest material in the Emerson Lake playa may be some sort of evaporite deposit. On the geologic map [16], there is no differentiation in the Emerson Lake playa deposit indicated. Melville Lake is almost indistinguishable in the imagery; it appears almost the same as the valley fill.

On the inspection of the S190B photograph, the Calico Fault and its extensions, the Johnson Fault, the Emerson Fault, and the Old Woman Springs Fault are evidenced by linear breaks in the surficial materials. See Figure 4.

4.2 RATIO PROCESSING OF S192 DATA

Twelve reels of S192 data of the Pisgah Crater area from the SL4 mission, Pass #91, were received. Table 1 gives the SDO's received and their corresponding band numbers and wavelength regions. Maps and screening film of the region were examined and boundaries of the study site were determined (see Figures 2 and 3).

With the study site defined, the data were edited down into a single reel (see Figure 5) which contained only the desired SDO's and the line and point coverage of the study site. Table 2 indicates the the eight selected SDO's and their corresponding band numbers and wavelength region.

Because of relatively large noise and electronic overshoot in the visible and near infrared channels, digital filtering was required before further processing.

The data were filtered using a digital filtering program written by Peter Lambeck of ERIM. The filtering program is designed to improve data quality by reducing and compensating for overshoot characteristics inherent in the X-5 detector array. During the filtering, it was discovered that SDO-4 (0.54 - 0.60 μm) was highly saturated and of very little use for this study.

Following the filtering of the data, the format was converted from Universal format to ERIM format to make the data compatible with ERIM's computer system.

Preliminary gray maps of a selected test site were prepared for all SDO's and used to check data quality. It was confirmed that SDO 4 was useless for this project. SDO's 8, 10, 12, 19 and 20 were found to be noisy but usable. SDO 14 had very little noise and had the best channel data quality of the eight SDO's considered.

A full gray map of the entire test area was prepared from SDO 8 for an examination of the area. Histograms were made for all channels in order to further check data quality and applicability, and to aid in determining parameters for ratio processing of selected channels. The

TABLE 1

PISGAH CRATER S192 DATA
RECEIVED FROM THE SL4 MISSION

SDO	Skylab Band Number	Wavelength (μm)
3, 4	4	.54 - .60
7, 8	6	.654 - .734
9, 10	7	.770 - .890
19	8	.930 - 1.050
20	9	1.030 - 1.190
11, 12	11	1.550 - 1.730
13, 14	12	2.10 - 2.34
21, 15, 16	13	10.2 - 12.5

TABLE 2

PISGAH CRATER S192 DATA
SELECTED FOR STUDY

SDO	Band Number	ERIM Channel Number	Wavelength (μm)
8	6	2	.654 - .734
10	7	3	.770 - .890
12	11	4	1.550 - 1.730
14	12	5	2.10 - 2.34
19	8	7	.930 - 1.050
20	9	8	1.030 - 1.190

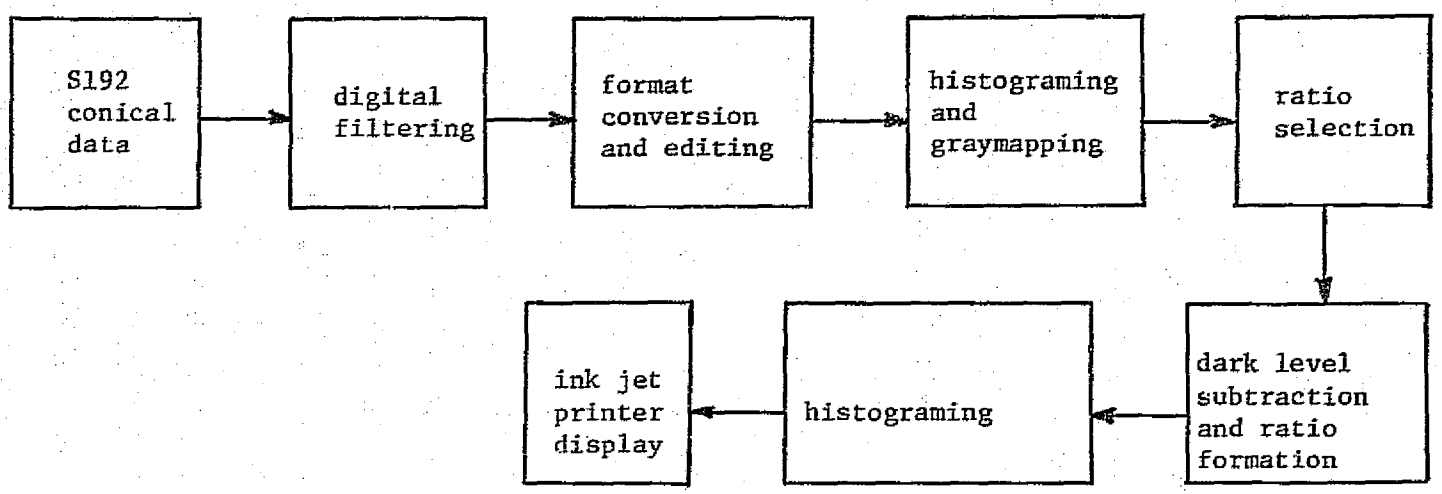

FIGURE 5. FLOW OF S192 RATIO PROCESSING OPERATIONS

histograms were used to select signal level intervals for gray scale definition in the production of test gray maps.

4.2.1 RATIO SELECTION

Iron compounds containing ferric iron generally exhibit high reflectances in the .77 μm and 1.5 μm wavelength regions and low reflectances in the .9 μm wavelength region. In a brief examination of example spectral curves of hematite, goethite, and limonite (Figure 6), relatively high reflectance values occur in the .77 - .80 μm wavelength region. Each of the curves exhibit low reflectance in the .90 - 1.0 μm wavelength region. High reflectance then occurs in the 1.5 μm wavelength region and the curve remains relatively flat or gradually decreases at wavelengths longer than 1.5 μm. The example curves of hematite, goethite, and limonite (all ferric iron containing minerals), agree with the generalizations made for ferric iron reflectance properties in Section 2.

The reflectance of ferrous iron gradually increases to peak in the .9 μm wavelength region, decreases to a low in the area around 1.0 μm and then starts to gradually increase beyond 1.0 μm. An example curve of weathered basalt (a ferrous iron containing rock) is included in Figure 6a. Its reflectance gradually increases to about .6 μm and then levels off and remains nearly constant after that. Basalt generally has a low reflectance. Weathered basalt does not exhibit the generalized reflectance characteristics for ferrous iron. This may possibly be due to weathering products that appear on the surface of the basalt.

Data quality and wavelength sensitivity were the major criteria used in selecting S192 bands for ratio processing. Bands 8, 7, 11, and 12 were the bands chosen to be used in the ratioing process. Band 8, .93 - 1.05 μm, is somewhat noisy. This band covers the wavelength region in which ferrous iron reflectance values are relatively high and ferric iron reflectance values are relatively low. Band 7, .77 - .89 μm, is

also noisy. A locally high reflectance for ferric iron containing materials occurs at .77 μm and is covered by band 7. Also somewhat noisy, band 11, 1.55 - 1.73 μm includes the main reflectance peak of ferric iron containing compounds. The spectral anomalies studied by Pohn [4] also appear in the 1.55 - 1.73 μm wavelength region. Band 12, 2.10 - 2.34 μm, has negligible noise and, where data quality is the main consideration, band 12 is the best S192 band available to this study.

Using the chosen S192 bands, the following ratios were selected to be examined in this study:

$$\frac{\text{Band 8}}{\text{Band 7}} = \frac{.93 - 1.05\ \mu m}{.77 - .89\ \mu m}$$

$$\frac{\text{Band 11}}{\text{Band 7}} = \frac{1.55 - 1.73\ \mu m}{.77 - .89\ \mu m}$$

$$\frac{\text{Band 12}}{\text{Band 11}} = \frac{2.10 - 2.34\ \mu m}{1.55 - 1.73\ \mu m}$$

Ratios 8/7 and 11/7 were chosen because they have the strong bands for differentiating ferric and ferrous materials. In Vincent's ratio ranking for differentiating silicate classes [22], ratio 8/7 was listed as the twelfth best ratio. Ratio 12/11 was selected for this study because it includes the best quality data band and one of the very good bands for possibly differentiating ferric materials. Vincent ranked the 12/11 ratio as the fifth best ratio for differentiating silicate classes.

4.2.2 RATIO PROCESSING

In ratio processing, some idea of the shape of the spectral response curve is obtained by taking the ratio of the radiance of an

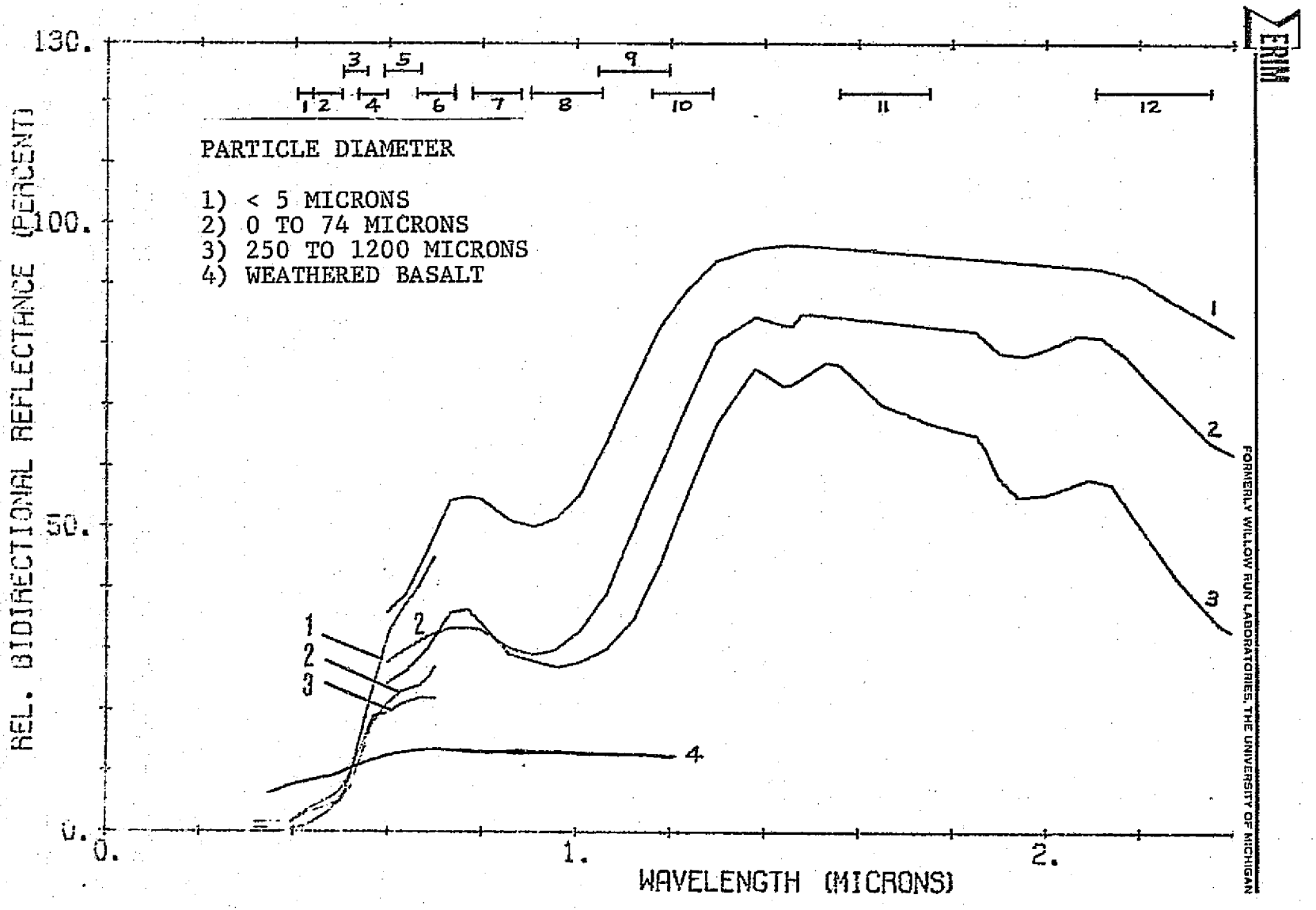

FIGURE 6a. SPECTRAL REFLECTANCE OF HEMATITE AND BASALT

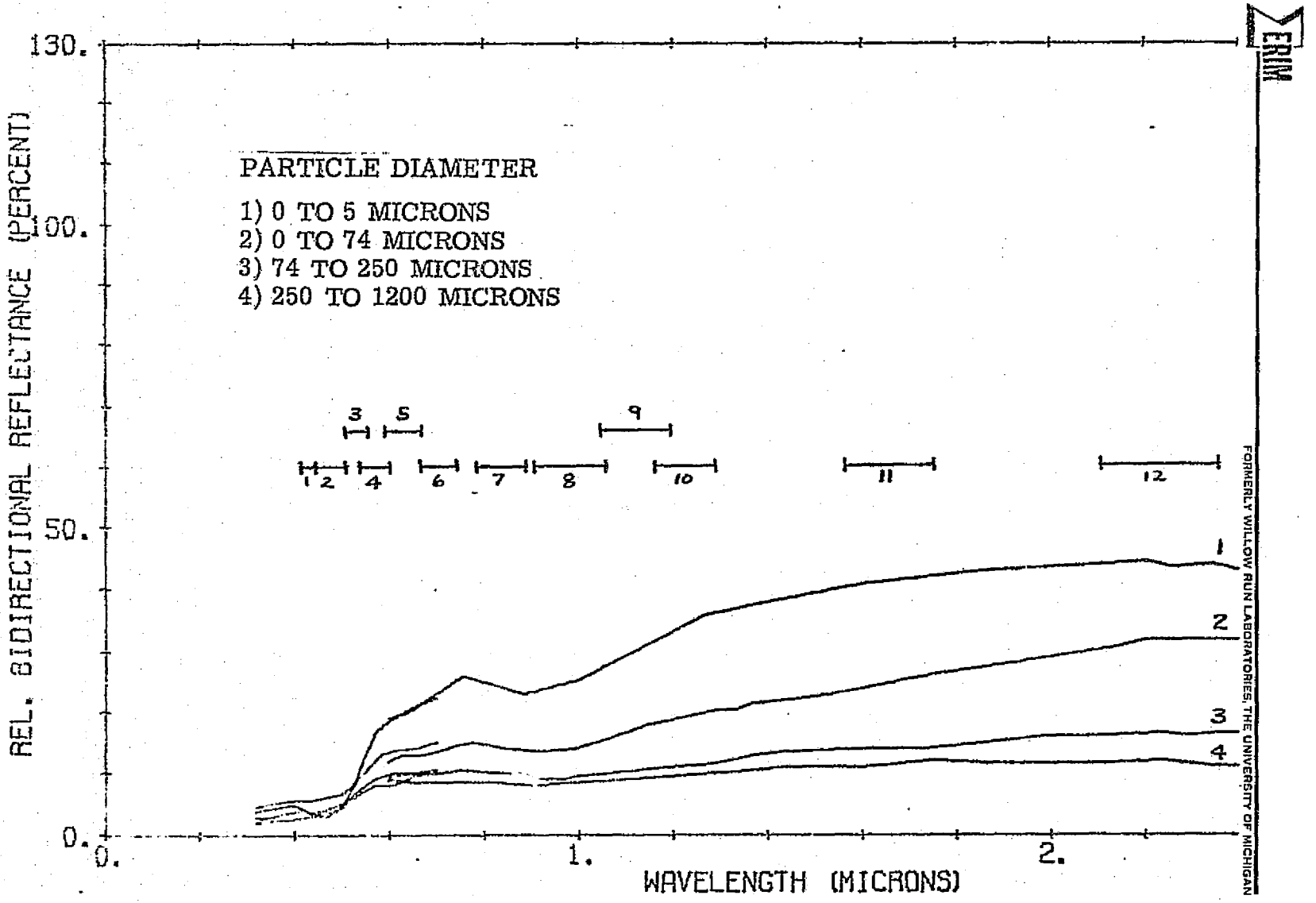

FIGURE 6b. SPECTRAL REFLECTANCE OF GOETHITE

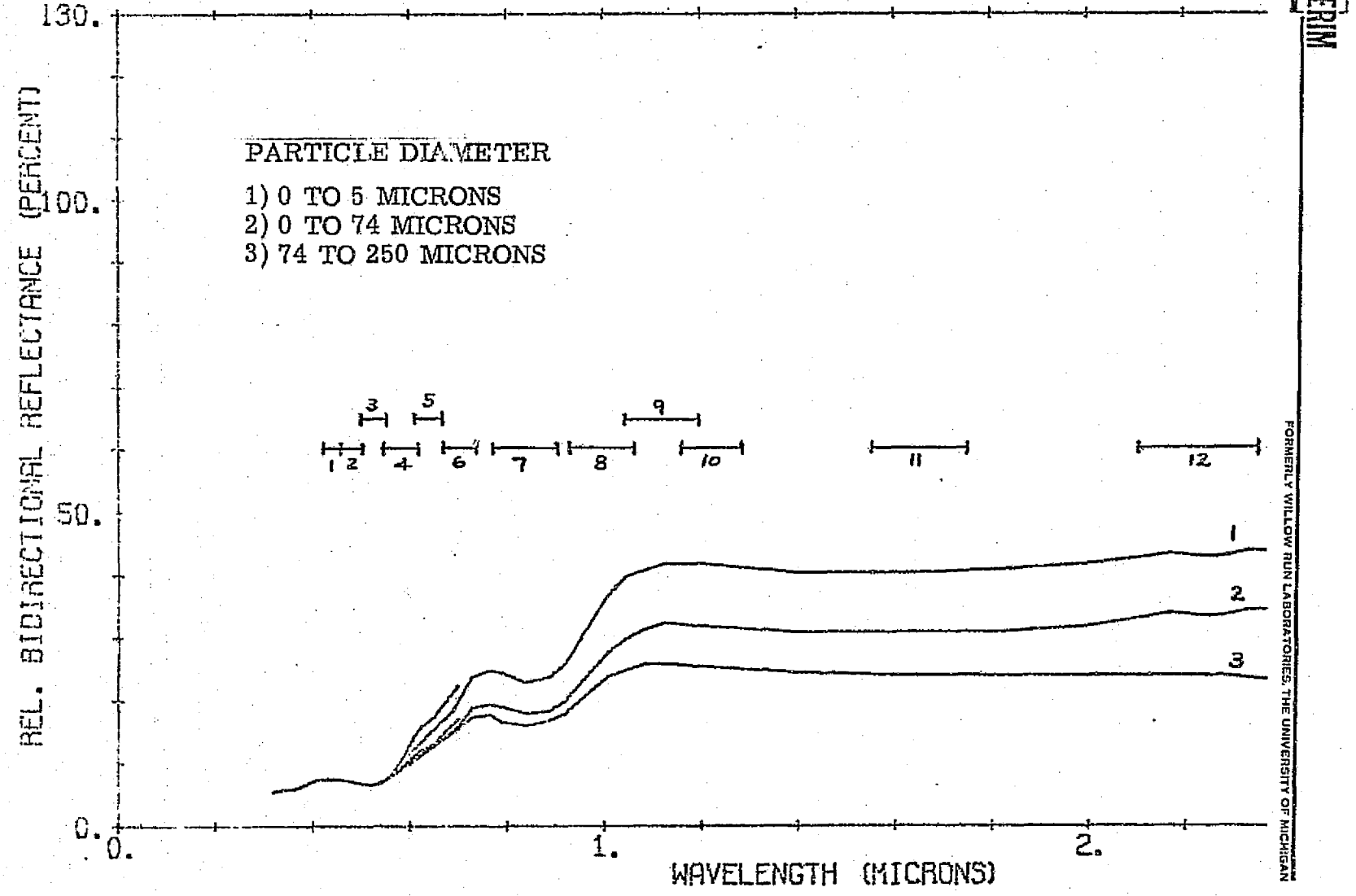

FIGURE 6c. SPECTRAL REFLECTANCE OF LIMONITE

object in one spectral band, and comparing it with the radiance of the same object in another spectral band. In order for this data to be meaningful, these values must represent only the radiance of the object in question, and cannot contain any radiance components from any other sources. For this to be accomplished, the path radiance must be subtracted from each value which will be used in the formation of a ratio. Path radiance may be estimated as the radiance of the darkest element in the scene. The path radiance is a constant for each spectral band, but it differs from band to band. This subtraction of path radiance is done on the single channels before they are ratioed. Once this subtraction has been done, theoretically, the ratio is being formed using only the reflected energy from the object under observation.

In the MSS processing programs at ERIM, the ratio data must be written in integer values on the tape. A scale factor is used to expand the range over which the values occur before they are converted to integer values and recorded on tape. The scale factor is a fixed multiplicative value applied to each ratio output before it is recorded. Its effect is to move the mean of the ratio values upscale by a factor approximately equal to the scale factor and to increase the width of the distribution of points occurring around the mean. If the scale factor is properly chosen, maximum use of the dynamic range of the ratio can be realized.

After the subtraction of path radiances from each band to be used in the ratioing and the determination of the scale factors for each ratio, the three selected ratios were generated. Histograms of radiance values in each ratio for selected training sites were prepared. From those histograms, signal level intervals were selected for the color scale definition for ink jet printer maps.

The three ratios, $\frac{.93 - 1.05}{.77 - .89}$, $\frac{1.55 - 1.73}{.77 - .89}$, $\frac{2.10 - 2.34}{1.55 - 1.73}$, and the one single channel which had been extensively gray-mapped .654 - .734, were prepared to be printed as ink jet printed maps. The resultant maps are shown in Figures 7-10.

4.3 ANALYSIS OF RESULTS

The purpose of processing the S192 data and photointerpreting the S190B data was to demonstrate what these processed data products could show in the scene. Enumeration of features of the processed data and comparison with the capabilities demonstrated with processed LANDSAT data are presented in this section. At the outset, we should mention that the approach taken in this section is not one of trying to pick the better sensor or processing technique. Rather we try to point out the advantages and disadvantages of the various types of processed data. It is likely that for any reconnaissance geologic investigation, both Skylab and LANDSAT processed data will be used, the exact mix depending on the application.

4.3.1 ANALYSIS OF S190B PROCESSED DATA

Maps of different colors of materials were made by photointerpreting S190B data. Basaltic areas were easily mapped because of their dark tones. The detrital and valley fill materials, as well as exposures of bedrock, are coated with weathering products containing ferric iron compounds, resulting in a characteristic red color of these materials throughout the imagery. This red color is frequently an indicator of iron-containing compounds. Because many of the formations in the area contain minerals such as biotite and magnetite, in which iron is a major constituent, it is possible, upon weathering, for a great deal of iron oxide to be produced, causing much of the surrounding material to become stained by red ferric oxide.

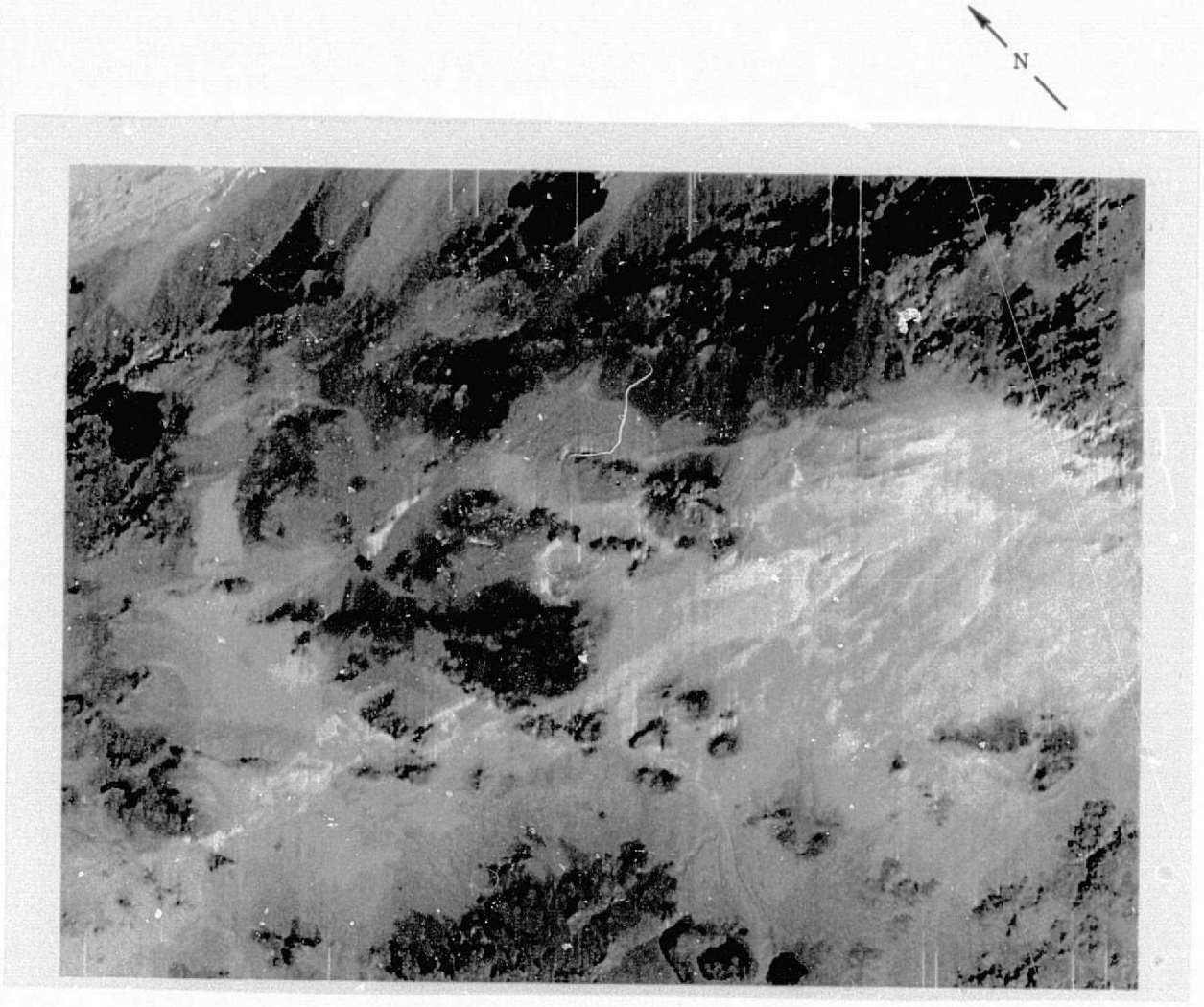

LEGEND

Black	Violet	Red	Orange	Yellow	White
Low Signal					High Signal

FIGURE 7. COLOR CODED DENSITY-SLICED SINGLE BAND S-192 IMAGE OF 50 × 30 st mi PISGAH CRATER TEST SITE (MSS BAND 6, CONICAL SCAN) 26 JANUARY 1974,1940 hrs GMT

FIGURE 8. COLOR CODED $R_{8/7}$ RATIO IMAGE OF 50 × 30 st mi PISGAH CRATER TEST SITE, 26 JANUARY 1974, 1940 hrs GMT

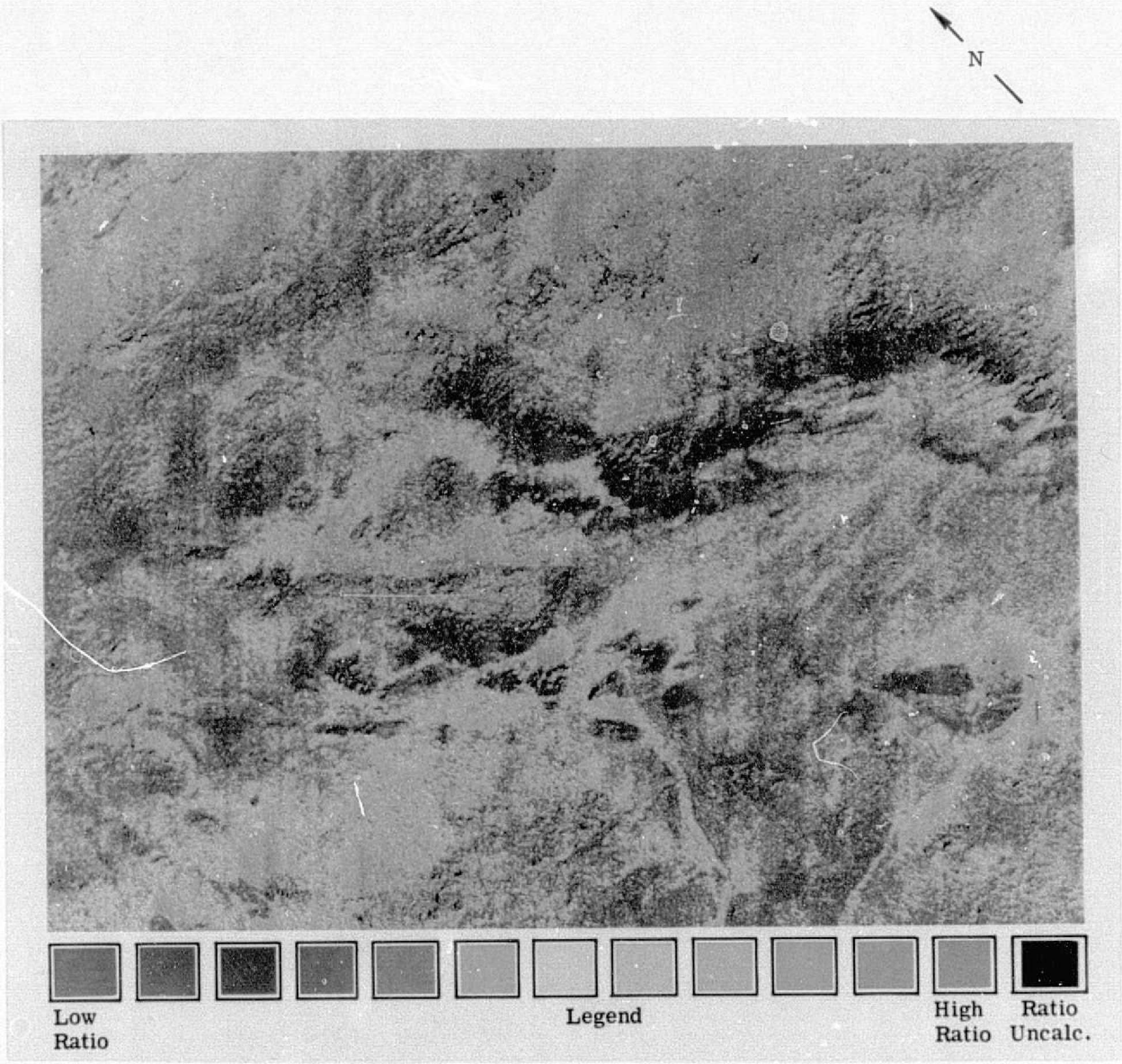

FIGURE 9. COLOR CODED $R_{12/11}$ RATIO IMAGE OF 50 × 30 st mi, PISGAH CRATER TEST SITE, 26 JANUARY 1974, 1940 hrs GMT

FIGURE 10. COLOR CODED $R_{11/7}$ RATIO IMAGE OF PISGAH CRATER TEST SITE, 26 JANUARY 1974, 1940 hrs GMT

The superiority of S190B imagery in this application is that it has potentially better resolution than LANDSAT, which means that geological interpretations on the basis of texture or fine color gradations of the rock exposures are more reliable. Also, because of this superior resolution, photography has the advantage of being more likely to discern small scale structural and textural features such as may be indicative of linear and fracture patterns.

S190B color photography may have some advantages over LANDSAT data for color mapping as well. In a study of LANDSAT data of the Wind River Basin, Salmon and Pillars [19] concluded that values of the ratio of LANDSAT bands 4 and 5 correlated most closely with Munsell hues from yellow to red. However, the ratio could not separate yellow and tan materials which appeared visibly different. The reason was that spectral reflectance differences between the yellow and tan samples occurred in the blue region of the spectrum, outside the response of LANDSAT channel MSS4. S190B color photography with its blue sensitive emulsion should be able to discriminate the yellow and tan samples, an important distinction to make for uranium exploration.

4.3.2 ANALYSIS OF S192 PROCESSED DATA

Color coded single channel and ratio maps were produced using a computer driven color ink jet printer at Mead Corporation, Dayton, Ohio. Color coding was determined through the use of histograms assuring a uniform distribution of data values within the color groups in each of the images produced.

4.3.2.1 Single Channel Image

A single channel color coded image was produced using SKYLAB Band 6 (see Figure 7). In this image, the relative radiance of data points was translated to a color scheme in which those points with the lowest radiance values were displayed in the darkest colors (black, dark blues, and violet). As the radiance value increased, brighter colors were chosen, many through reds, orange, and yellow to white.

Band 6 was chosen for this purpose, because of the available data, it was in the middle of the visible spectrum, permitting a more direct comparison of this technique with manual interpretation of conventional photography.

An interpretation of this image indicates that, in general, the different geologic units occurring in the study area were distinguished by this method and are represented on the image by different colors; Basalts by black, acidic silicate rocks by blues, weathering products derived from these rock outcrops by reds and oranges and salt and evaporite deposits in Playa Lake basins and in the floors of valleys as the brightest yellows and whites. The reliability of this classification, though generally good, is compromised by terrain slope and illumination effects. Since radiance is determined both by reflectance and slope relative to the position of the sun, a significant variation in either factor will cause a color shift to be produced in this image. Consequently, there are several areas in which acidic rocks are imaged in black, not because of the presence of more mafic materials, but rather because of sun angle/shadow effects.

In general the boundaries between areas of differing lithologies that were determined by this method correspond to a high degree to those produced manually using S190B imagery as the basis for photogeologic interpretation. Drainage patterns are visible at several places within the test area, possibly due to slightly different optical properties of the detritus within these systems, possibly due to differing soil moisture content compared with the areas surrounding them, or both.

An interpretation of this image on the basis of ferric and ferrous iron is possible with a knowledge of the area and field study. Ferrous iron, as represented by quartz monzonite and basalt outcrops appears as the darker colors, blues, purples, and blacks. Ferric iron of the weathered sediments is indicated by reds and oranges. This differentiation is similar to that obtainable from examination of S190B data,

although this method may be somewhat more dependent on ground truth information then is the interpretation of S190B imagery.

4.3.2.2 Ratio Images

Three color coded ratio images were prepared in a manner similar to that used in the single channel image described in the previous section. In these images, the color printed was determined by the magnitude of the scaled value produced by the ratioing of two channels at each point. In general, all of the ratio images produced have a coarse speckled texture when compared to the single channel image. This decrease in image quality is caused by the ratio processing. The result of this noise is a decrease in the resolution of the imagery when compared to a single channel and an accentuation of scan line and electrical overshoot problems found in some of the channels of data used. The problem was most prevalent in the ratios of all band 8/7 and 11/7 where due to the accentuation of overshoot characteristics of the detectors large areas were mis-coded in the color ratio imagery. This could have caused incorrect interpretation of results had the effect not been detected and compensated during the interpretation of data.

The ratio process produces images which are much less succeptible to variations in illumination and terrain than are single channel images. This increases their usefulness in the classification of materials due to reflectance characteristics. This effect is well illustrated in the ratio images produced, but is masked somewhat by the electronic overshoot characteristics which are found in the images.

In general, the $R_{8,7}$ ratio image (the ratio of 0.93 - 1.05 and 0.77 - 0.89 μm bands) appears to seperate three classes of materials, based on ferric and ferrous iron content (see Figure 8). The basaltic rocks in the test site are imaged in blue, indicating a low ratio value, which, in this ratio, should be indicative of ferrous compounds.

Similarly, the acidic rocks are imaged in blue, because of ferrous iron content. The pink colors associated with some of the Quartz Monzonites, especially in the area of the Bullion Mountain, is explained by electronic overshoot in the preamplifiers, and does not represent a different class for these rocks.

The sediments which flank the slopes of the highlands are imaged in reds and oranges which indicates the highest ratio values (exclusive of the overshoot), and valley floor sediments imaged in yellow and green, indicating some intermediate values.

From the above observations, it can be seen that it is difficult to distinguish between granitic and basaltic rocks in outcrops. Indeed, since they both contain ferrous iron, differentiation between these rock types is not necessarily desirable within the context of this study. These rock types are, however, easily differentiated from the weathered sediments which flank them. We believe this possibly represents a successful discrimination between ferrous and ferric iron. As the concentration of ferric iron decreases in the surficial deposits of the valley floors, the colors produced in the image shift towards yellows and greens. This is interpreted as a differentiation between ferric and non-ferric containing detrital materials.

It is therefore believed that this ratio is capable of producing a unique three member discrimination between ferric, ferrous, and non-iron containing surficial materials.

The overall sensitivity of this ratio to illumination differences is fairly low, and can be measured indirectly by comparison with Figure 7. In Figure 7, the valley to the southeast of Emerson Lake contains several highly reflective areas, possibly due to superficial evaporite deposits. In the ratio image, this area is generally of a uniform tone.

Of the ratio images studied, the $R_{12,11}$ image (the ratio of 2.05 - 2.34 and 1.55 - 1.75 μm bands) shows the least speckle noise and overshoot (see Figure 9).

In this image, the basaltic rocks on the northern edge of the imagery produce a pink response indicating a very high level ratio signal, which agrees with theory, since ferrous iron should produce a high response relative not only to ferric iron, but also to clay and evaporite materials as well. The weathered sediments flanking the northern highlands produce a green response, which in this ratio is believed to indicate the presence of ferric iron. The sediments of the valley floors are imaged in a range of colors from greens to reds. These sediments decrease surficially in ferric iron as the distance from the highlands increase. The acidic rocks which occur in the area are imaged in blue.

This image is interpreted as basically discriminating between ferric and non-ferric materials. Since the difference between the ratio values of ferric and ferrous containing materials is fairly low for this pair of bands, other materials such as clay and carbonates have a significant effect upon the ratio values obtained. A discrimination can be made between mafic rocks, which generally produced high (pink) ratio values and acidic rocks which produced low (blue) ratio values. The sediments containing a high ferric content have been images in this ratio in a green color. As the concentration of ferric iron in the sediments decreases, the concentrations of other materials control ratio values, producing either yellows and reds or blue colors in Figure 7. This is dependent on the material causing the displacement.

The basaltic rocks of the Little San Bernadino Mountains are portrayed in different colors than the basalts that occur to the north such as those from the Malpais Crater Flow. The Little San Bernadino basalts are portrayed in the same color as the more acidic Quartz Monzonites that occur in the test area. The Little San Bernadino

basalts are of a different age than the ones to the north — Pliocene rather than Pleistocene. Although an inspection of the geologic maps revealed no major differences in mineralogy between the basalts, the different ratio values of the Little San Bernadino basalts may be caused by either a lower concentration of ferrous iron bearing minerals and/or a high concentration of ferric minerals or to different weathering characteristics which produce a higher amount of surifical ferric ion staining.

The interpretation of the $R_{11,7}$ (the ratio of 1.55 - 1.75 and 0.77 - 0.89 μm bands) is complicated by the presence of overshoot and/or clipping problems in the data (see Figure 10). This problem occurs where a combination of sun angle and terrain geometry cause a high level specular reflection. This apparently caused clipping in channel 7, producing a false high level ratio signal to be produced everywhere that this problem occurred. The most widespread occurrence of this problem is in the Quartz Monzonites in the northeastern corner of the image, but can be noted in several other places throughout the image.

The theoretical analysis of this ratio indicates that ferrous compounds should produce a low response, ferric compounds a high response, and non-iron containing materials a low to intermediate response. Except for those regions affected by the clipping problem, this relationship has been found to hold true.

The basaltic and acidic rock outcrops are generally in blue, and the sediments flanking the highlands range in color from reds and oranges through yellows and greens. It is believed that this shows the varying concentrations of ferric iron with a marked decrease towards the valley floors.

This ratio appears more susceptible to illumination effects than the other images analyzed, perhaps because of the relatively large spectral separation of the ratio channels. This could be one reason for the somewhat different classification of the sediments between Copper and Hidalgo Mountains when compared with the $R_{8,7}$ image of the same area.

A review of the success of the three ratio images studied with regard to ferric/ferrous discrimination indicates that of the ratios studied $R_{8,7}$ appears to be the best suited for the purpose, $R_{11,7}$ intermediate, and $R_{12,11}$ least suited. It should be noted that the channels used for the formation of the ratios used did not represent an optimal channel selection due to the lack of availability of data. The results are consistent with theoretical predictions made about the utility of splitting up the LANDSAT MSS7 band [11]. A ratio of 0.77 - 0.89 and 0.93 - 1.05 μm bands was found most useful for ferrous-ferric iron discrimination, consistent with the location of ferrous and ferric iron absorption features at 1.0 and 0.87 μm respectively.

4.3.2.3 Faults and Linear Features on Processed S192 Data

The study site is cut by a system of faults which are generally parallel and are aligned Southeast-Northwest. An inspection of S190B imagery indicates that although these structures are not always obvious on first inspection, they can usually be traced on the imagery for long distances, and can at times be exactly located where they have been mapped as only approximately located or concealed.

The color coded images examined for this project appear to be at least as useful for the detection and mapping of linear features as photographic imagery, and there are indications that they may indeed be more useful. Because many of the faults in the study area mark the boundaries between different rock types, they are usually delineated on the color coded ratio imagery by an abrupt and sometimes major color

shift. This color shift occurs in a straight line which indicates the trace of the fault intersection with the surface of the ground. These features are most obvious on the $R_{12,11}$ and $R_{11,7}$ images formed for this study. An example which can be used for comparison is the Emerson Fault which runs generally parallel to the regional trend, and is most obvious on the imagery just south of Emerson Lake.

An interesting finding of this study is seen in the $R_{11,7}$ image to the Southeast of the Bullion Mountains. Here, the Mesquite Fault is buried beneath Recent Alluvium. Although it is concealed and was mapped that way by ground surveys, a short section of it appears as a blue line segment against the orange and yellow alluvium. This emphasis of the fault may possibly be due to drainage or compositional differences in the deposits directly overlying the fault. It is believed that processing options could be modified to enhance detection of these features should it prove desirable to do so.

5

ANALYSIS OF S191 DATA TO DETERMINE THE FEASIBILITY OF MAPPING SILICATE COMPOUNDS

Silicates are an important class of minerals for both general geologic mapping and for more focussed mapping tasks associated with location of ores. Thus an ability to map silicate minerals as a class separate from the non-silicates, or to differentiate between various silicates on the basis of compositional variations in an important capability for the geologist.

Section 2 presented some previous work on the feasibility of mapping silicates using spectral emissivity differences (caused by reststrahlen) in the 8 - 12 μm region of the spectrum. In this section, we discuss the analysis of S191 data collected over basalt and dacite within the Pisgah Crater Test Site. The goals were to determine if the basalt and dacite could be separated using spectral emissivity information collected by S191, and to determine good spectral bands and the sensor radiometric precision (noise equivalent temperature, NET) necessary for separation of the two rock types.

5.1 ANALYSIS OF S191 DATA

Figure 11 shows the processing steps followed for the analysis of S191 data, supplied on computer-compatible tape.

As a first step, we processed the S191 tapes through a program written for the IBM 370/168 computer to reconstruct calibrated data, create a listing of radiance versus wavelength with continuously increasing wavelength, and to punch cards compatible with the ERSIS library.

Spectra were selected for study by an examination of the boresight 16mm film supplied along with the computer-compatible tape. Spectra were selected for the basalt and for dacite. Several spectra which covered boundaries between basalt and alluvium were discarded. The result was nine spectra for basalt and three for dacite.

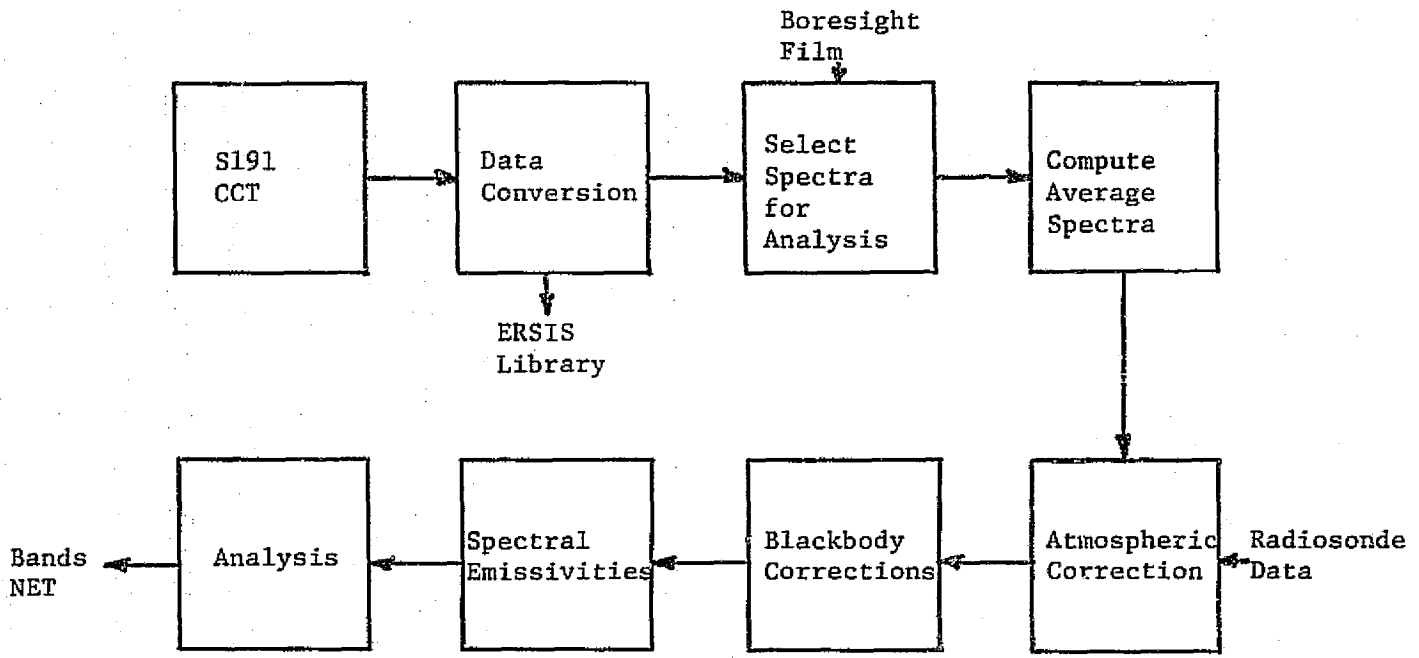

FIGURE 11. FLOW OF PROCESSING FOR STUDY OF S191 DATA FROM PISGAH CRATER TEST SITE.

Average spectra were then computed as a function of wavelength for the range 8 - 12.0 μm. The spectral resolution of the S191 data in this region is 0.1 μm. Before further analysis could be completed, corrections for atmospheric effects had to be made. The atmospheric transmission and path radiance were calculated by a computer program developed at ERIM by Anding, Rose, and Turner [21]. The program accounts for absorption and re-emission of carbon dioxide, water vapor, ozone, and aerosols. As input to the model to define the atmospheric conditions, we used radiosonde vertical temperature and humidity profile data measured at Yucca Flat, Nevada at 0000 hrs GMT on 27 January 1974 — about 4 hours after the S191 overpass at 2000 hrs GMT on 26 January 1974. The radiosonde data were obtained from the National Weather Records Center in Asheville, North Carolina. The radiosonde data used were the closest available in space and time and were felt to be more accurate than the standard profiles assumed by the model in the absence of radiosonde data.

The average spectral radiance data for basalt and dacite were corrected by subtracting the computed path radiance and dividing by the transmission in order to obtain the radiance from the two materials at the surface. There was evidence that the temperature profile at 0000 GMT (about 4 p.m. in the afternoon) was different from that at noon. We concluded this after an examination of corrected radiance values revealed anomalously large values around 8.0 μm and in the ozone band at 9.5 μm, where absorption and path radiance were greatest. Effects of this sort could be caused by path radiances or path transmission which were too small. Since path transmission depends on the vertical distribution of water vapor (primarily), while path radiance depends on not only the vertical distribution but the vertical temperature profile as well, the chances are more likely that the path radiance term is in error. The effect was most pronounced in the absorption bands. Since data in this region would not be typically used for remote sensing applications, the

problems in those regions is not serious. However, insofar as anomalous values of spectral radiance there may imply problems with the corrected spectral radiance at other wavelengths, results at those wavelengths should be viewed with caution.

To compute spectral emissivities for basalt and dacite, corrections for the different temperatures of the two materials was made. In the region around 12 μm, most silicates have uniform emissivity, which in this case was assumed to be 1.0. An equivalent blackbody temperature was computed from the spectral radiance at 12.0 μm for both materials. Then the spectral radiances for the materials at other wavelengths were divided by the blackbody radiance at the appropriate temperature to yield the spectral emissivity. Table 3 shows the spectral emissivities for basalt and dacite, respectively. The absolute values of the emissivity are less than what would be expected from the laboratory data for reasons which have already been discussed. But the relative emissivities between basalt and dacite, as well as the relative values on the short wavelength side of the ozone absorbtion compared to those on the long wavelength side, appear to be correct. Hence the conclusions drawn later about the ratio processing appear to be justified.

After the spectral emissivities have been obtained, ratios of the emissivities were formed. Before dividing, the emissivities were averaged over bands corresponding to the sensitivity of the Surface Composition Mapping Radiometer and over bands selected as optimum by Robert Vincent [3]. The emissivity ratios are shown in Table 4. To obtain these values, the average emissivity in the short wavelength band was divided by the average emissivity in the long wavelength band. The emissivity ratios for basalt and dacite are different for both band configurations, indicating that these materials can be separated with the band ratio technique. Approximately the same difference between the basalt and dacite ratios occur for the two sets of bands.

TABLE 3

SPECTRAL EMISSIVITY FOR BASALT AND DACITE
COMPUTED FROM S191 DATA

Wavelength (μm)	Basalt Emissivity	Dacite Emissivity
8.2	.7374	.7255
8.3	.6901	.6772
8.4	.7417	.7256
8.5	.7417	.7242
8.6	.7314	.7236
8.7	.7437	.7276
8.8	.7326	.7114
8.9	.7260	.7070
9.0	.7297	.7239
9.1	.7308	.7140
9.2	.7223	.7238
9.3	.6740	.6806
10.2	.8723	.8710
10.3	.8394	.8345
10.4	.8458	.8507
10.5	.8571	.8560
10.6	.8701	.8781
10.7	.8793	.8890
10.8	.8833	.8979
10.9	.8927	.9082
11.0	.9005	.9160
11.1	.9119	.9308
11.2	.9204	.9305

TABLE 4

SPECTRAL EMISSIVITY RATIO VALUES
FOR BASALT AND DACITE

	Basalt	Dacite
Vincent Optimum Bands 8.3 - 8.8 and 10.3 - 10.8 μm	.847	.824
SCMR Bands 8.3 - 9.3 and 10.2 - 11.2 μm	.824	.803

5.2 SILICATE ROCK MAPPING SYSTEM IMPLICATIONS

The S191 data can be used to specify both good spectral bands and the radiometric performance required of a sensor to distinguish basalt from dacite. From the foregoing analysis we can see that either the 0.5 μm wide Vincent optimum bands or the 1 μm wide SCMR bands (simulated from S191 data) show about the same difference in ratio value for basalt and dacite. But under realistic sensor noise conditions the ratios computed over basalt and dacite will be noisy and the ratios can be separated only if the difference exceeds the noise level by a sufficient amount. If we assume that the ratio values can be separated when their difference equals the standard deviation of the noise, then the required NET can be computed.

When these computations are made, we find an NET of 1.2°K for the Vincent bands and 1.1°K for the SCMR bands. A sensor with this level of performance or better will be able to separate the two materials.

The need for a third band for estimating the temperature of ground materials arises from the fact that changes of temperature cause radiance ratio changes just as changes in spectral emissivity do. If we can measure the temperature of ground objects in a band from 12.0 - 12.5 μm where silicates have uniform emissivity, corrections to the radiance ratio can be made. As an example of the effect of temperature on the ratio values, a change of temperature of dacite from 292°K to 300°K will make the radiance ratio of dacite equal to that of basalt [2]. Temperature measurements should be done with an accuracy better than this 8°K difference in temperatures. A 1°K NET for the third channel would be a good choice.

6
CONCLUSIONS

As a result of these investigations, several conclusions were reached. They are summarized in Section 1.3 of this report and disucssed in more detail in this section.

6.1 S190B PHOTOGRAPHY

The S190B color photography was found at least as useful as LANDSAT for mapping color differences in terrain. When we speak of color difference mapping we do not typically use the infrared bands of the LANDSAT sensor. The improved S190B capability partly stemmed from the presence of the blue emulsion of the S190B color photography and partly from the improved spatial resolution of the S190B imagery. The improved spatial resolution allowed the photointerpreter to make distinctions based on tone and texture, and thus to map more categories in the and, relatively vegetation-free terrain around Pisgah Crater California. An added advantage of the better spatial resolution of the S190B sensor was the ability to more precisely locate and trace fault lines.

There was evidence from another study that the LANDSAT $R_{5,4}$ ratio data could not be used to discriminate between yellow and tan colored rocks in the Wind River Basin of Wyoming. The reason for this is that differences in reflectance signatures for the tan and yellow materials occurred in the blue region of the spectrum, around 0.48 μm [19]. The S190B sensor, with the blue sensitive emulsion could potentially be used to make this distinction, important in the location of uranium-bearing minerals.

The one disadvantage of the S190B is the limited coverage obtained. LANDSAT data are available for nearly the entire globe on a repeatable basis. S190B imagery has been collected over much smaller areas and maybe only once for many of those areas.

6.2 UTILITY OF SPECTRAL RATIO IMAGES

We feel that spectral ratio images, presented as black and white images, as color composites, or as color density sliced images, are a useful tool for geologic interpretation. When the pairs of bands are selected from an analysis of laboratory data to maximize the contrast between e.g., ferrous and ferric iron features, and the remote sensor data are properly preprocessed to reduce the contribution from the atmosphere, the ratio can display new features of the terrain such as surface composition variations. Ratio images, in and of themselves, are not the only source of information needed to form an accurate picture of the geology of an area, but they are important pieces of information.

6.3 COMPARISON OF LANDSAT AND S192 RATIO IMAGERY

A detailed comparison of S192 and LANDSAT spectral ratio capability was not possible because data from only eight of the thirteen S192 bands were usable. The missing channels in the blue and green regions precluded a study of optimizing the information portrayed in LANDSAT ratio $R_{5:4}$. The five channels were missing from the S192 data because the data were collected with the X-5 detector array. This array was optimized for thermal sensitivity, and most of the visible channel showed high noise levels and overshoot caused by mismatch of the preamplifier and detector frequency response. NASA judged the quality of S192 bands 1-3 to be not worth processing further, and these data were not supplied to ERIM. The remaining channels required extensive digital filtering to bring the overshoot within tolerable levels.

An S192 ratio map using 0.77 - 0.89 and 0.93 - 1.05 μm bands apparently successfully delineated ferric and ferrous compounds. This performance was predicted from an examination of the spectral curves of various ferrous and ferric iron containing minerals and from the resultant ratio codes. The discrimination occurs because of the presence

of absorbition features of ferric iron at 0.87 μm in the short wavelength band and absorbtion features of ferrous iron at 1.0 m in the long wavelength band.

This type of discrimination could not have been obtained with LANDSAT data because the spectral response of the MSS7 band is too broad (0.8 - 1.1 μm). To the extent that the distinction between ferric and ferrous iron content of the surface is an important indicator for geologic applications, this S192 capability is an important advance over the LANDSAT capability. It is recommended that bands in this region of the spectrum be considered for future sensors for geologic applications.

6.4 DELINEATION OF SILICATE MINERALS BY RESTSTRAHLEN TECHNIQUES

We found by examination of S191 spectrometer data collected over Pisgah Crater, that basalt and dacite could be separated on the basis of spectral emissivity differences in the 8.3 - 12 μm region of the spectrum. A temperature corrected radiance ratio algorithm, previously developed by Vincent and Thomson [1] was used. An analysis of the contributions of noise to ratio uncertainty led to the requirement of a 1°K NET performance for either of two band sets — two optimum 0.5 μm wide bands originally investigated by Vincent [2] and then two 1 μm wide bands of the NIMBUS-5 Surface Composition Mapping Radiometer.

An analysis of the effects of temperature changes on the two band radiance ratio leads to the requirement for a third band, of approximately the same performance as the first two. A suitable wavelength response for this third channel would be 12.0 - 12.5 μm, where the emissivities of most silicate-containing rocks are nearly the same. Failing to correct for temperature variations between different rock types may render decisions based on the radiance ratio ambiguous Correction for atmospheric transmission and path radiance should also be made for best results.

REFERENCES

1. R. K. Vincent and F. J. Thomson, "Rock Type Discrimination from Ratioed Infrared Scanner Images of Pisgah Crater, California," Science, vol. 175, pp. 986-988, March 1972.

2. R. K. Vincent, R. Horvath, F. Thomson, and E. A. Work, "Remote Sensing Data-Analysis Projects Associated with the NASA Earth Resources Spectra Information System," Report 3165-26-T, Environmental Research Institute of Michigan, Ann Arbor, Michigan, April 1971.

3. L. C. Rowan, "Near-Infrared Iron Absorption Bands: Applications to Geologic Mapping and Mineral Exploration," in Fourth Annual Earth Resources Program Review, NASA, Johnson Space Center, Houston, Texas, January 1972.

4. H. A. Pohn, "Near-Infrared Reflectance Anomalies of Andesite and Basalt in Southern California and Nevada," Geology, pp. 547-550, November 1974.

5. G. R. Hunt, J. W. Salisburry, and C. J. Lenhoff, "Visible and Near-Infrared Spectra of Minerals and Rocks. VII Acidic Igneous Rocks," Modern Geology, vol. 4, pp. 217-224, 1973.

6. _____, "Visible and Near-Infrared Spectra of Minerals and Rocks: VIII Intermediate Igneous Rocks," Modern Geology, vol. 4, pp. 237-244, 1973.

7. _____, "Visible and Near-Infrared Spectra of Minerals and Rocks: IX Basic and Ultrabasic Igneous Rocks," Modern Geology, vol. 5, pp. 15-22, 1974.

8. J. W. Salisburry and G. R. Hunt, "Remote Sensing of Rock Type in the Visible and Near-Infrared," in Ninth Symposium on Remote Sensing of Environment, Environmental Research Institute of Michigan, Ann Arbor, Michigan, pp. 1953-1958, April 1974.

9. R. K. Vincent, "A Thermal Infrared Ratio Imaging Method for Mapping Compositional Variations Among Silicate Rock Types," Ph.D. Dissertation, Department of Geology and Mineralogy, University of Michigan, Ann Arbor, Michigan, 1973.

10. R. J. P. Lyon, "Evaluation of Infrared Spectrophotometry for Compositional Analysis of Lunar and Planetary Soils: Rough and Powdered Surfaces," Final Report, Part 2, NASA-CR-100, 1964.

11. S. J. Garvarecki, "Infrared Survey of the Pisgah Cr. er Area, San Bernadino County California: A Geologic Interpretation," NASA-CR-99234, January 1969.

12. T. W. Dibblee, Jr., "U.S.G.S. Miscellaneous Geological Inventory Map I-426," 1964.

13. _____, "U.S.G.S. Miscellaneous Geological Inventory Map I-430," 1964.

14. _____, "U.S.G.S. Miscellaneous Geological Inventory Map I-472," 1966.

15. _____, "U.S.G.S. Miscellaneous Geological Inventory Map I-488," 1967.

16. _____, "U.S.G.S. Miscellaneous Geological Inventory Map I-490," 1967.

17. _____, "U.S.G.S. Miscellaneous Geological Inventory Map I-517," 1967.

18. _____, "U.S.G.S. Miscellaneous Geological Inventory Map I-518," 1967.

19. B. C. Salmon and W. W. Pillars, "Multispectral Processing of ERTS-A (LANDSAT) Data for Uranium Exploration in the Wind River Basin, Wyoming," Report 110400-2-F, Environmental Research Institute of Michigan, Ann Arbor, Michigan, August 1975.

20. L. C. Rowan, P. H. Wetlaufer, A. F. H. Goetz, Jr., F. C. Billingsley, and J. H. Stewart, "Discrimination of Rock Types and Detection of Hydrothermally Altered Areas in South-Central Nevada by the use of Computer-Enhanced ERTS Images," U.S. Geological Survey Professional Paper 883.

21. D. C. Anding, H. Rose, and R. E. Turner, "Atmospheric Effects on Infrared Multispectral Sensing of Sea Surface Temperature from Space," Report 2676-6-F, Environmental Research Institute of Michigan, Ann Arbor, Michigan, December 1970.

22. R. K. Vincent and W.W. Pillars, "Skylab S-192 Ratio Codes of Soil, Mineral, and Rock Spectra for Ratio Image Selection and Interpretation," in Proceedings of the Ninth Symposium on Remote Sensing of Environment, Environmental Research Institute of Michigan, Ann Arbor, Michigan, April 1974.